

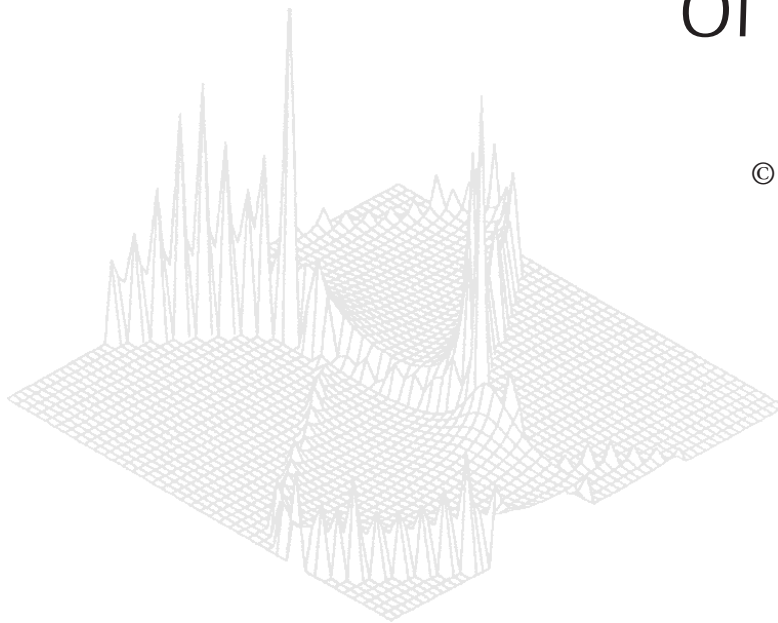
---

CSIRO PUBLISHING

---

# Australian Journal of Physics

Volume 50, 1997  
© CSIRO Australia 1997



A journal for the publication of  
original research in all branches of physics

[www.publish.csiro.au/journals/ajp](http://www.publish.csiro.au/journals/ajp)

All enquiries and manuscripts should be directed to

*Australian Journal of Physics*

**CSIRO PUBLISHING**

PO Box 1139 (150 Oxford St)

Collingwood

Vic. 3066

Australia

Telephone: 61 3 9662 7626

Facsimile: 61 3 9662 7611

Email: [peter.robertson@publish.csiro.au](mailto:peter.robertson@publish.csiro.au)



Published by **CSIRO PUBLISHING**  
for CSIRO Australia and  
the Australian Academy of Science



## Neutron Polarisation Analysis, Spin Glasses and Other Systems\*

*T. J. Hicks*

Department of Physics, Monash University,  
Clayton, Vic. 3168, Australia.

### *Abstract*

This paper describes neutron scattering experiments on a spin glass, Cu–Mn, an inhomogeneous antiferromagnetic alloy,  $\gamma$ -Mn–Ni, and the crystal field excitations in PrAl<sub>3</sub>. In all materials the magnetic part of the scattering has been isolated using polarisation analysis with the long wavelength polarised neutron diffractometer–spectrometer (LONGPOL) installed at the HIFAR reactor at Lucas Heights.

### **1. Introduction**

Neutron scattering is a very useful tool for revealing the underlying magnetic state of materials and it is made even more potent when polarisation analysis is used to definitively separate the magnetic part of the scattering. Neutron scattering (Ahmed and Hicks 1974) directly confirmed the magnetic glassiness of materials dubbed as spin glasses (Coles 1970) from their bulk magnetic properties. Models which describe the magnetic susceptibility of spin glasses are also useful for the description of neutron scattering because of the intimate relationship between susceptibility and the neutron cross section. Neutron scattering has also characterised the inhomogeneities in magnetic moment in ferromagnetic and antiferromagnetic alloys (Hicks 1995). In both of these cases, examples of which will be discussed in this paper, the magnetic neutron scattering is diffuse and polarisation analysis is necessary to identify it.

Not only is neutron scattering capable of revealing the spatial arrangement of magnetic moment, it is also able to measure magnetic dynamics such as collective excitations like magnons and the magnetic transitions in individual magnetic atoms. The former are characterised by definite wave-vectors and energies and are easily distinguished in energy dependent neutron scattering, while the latter are widely dispersed in wave-vector space but with definite energies. Neutron polarisation analysis is useful for isolating the latter from other energetically sharp excitations.

\* Refereed paper based on a contribution to the Sixth Gordon Godfrey Workshop on Recent Developments in Magnetism and Magnetic Materials, held at the University of New South Wales, Sydney, in October 1996.

Magnetic problems, such as these, require neutron instruments which have a capability beyond that of mere diffraction. The long wavelength polarised neutron diffractometer–spectrometer (LONGPOL) installed at the HIFAR reactor at Lucas Heights is one such which has been successful in probing these more sophisticated magnetic problems. Its capabilities include the ability to measure magnetic and atomic correlations and the energies of magnetic excitations, and it does this with neutron polarisation analysis so that quantitative measurements can be made of both the magnetic and nuclear intensities from materials. All but one of the investigations described in this paper have been done using LONGPOL.

## 2. LONGPOL

The practice of neutron polarisation analysis has taken a number of different forms. The simplest of these is based on the workhorse of neutron scattering, the triple axis spectrometer. In this instrument the first axis carries a crystal which serves as a neutron monochromator. The second axis carries the sample and the third axis carries a crystal which serves again as a monochromator, but in this case is selecting from the range of wavelengths which result from inelastic scattering in the specimen. To equip a triple axis for neutron polarisation analysis simply requires the first and third axes to carry crystals which polarise the beam as well as monochromate. LONGPOL, in contrast, uses polarising and analysing filters with the monochromation done separately. This has the advantage of allowing the monochromation to be relaxed and the intensity increased. However, this is only useful if lax monochromation can be tolerated and LONGPOL has been used historically for measurements of diffuse scattering for which high resolution is not necessary.

Fig. 1 is a schematic drawing of LONGPOL in its present configuration. The beam is monochromated by a pair of pyrolytic graphite monochromators arranged in a dog-leg configuration. Because of their large mosaic spread, these deliver a  $3.6 \text{ \AA}$  beam with a wavelength spread of 8% FWHM. Significant amounts of  $1.8 \text{ \AA}$  and other lower order contaminants are removed by blocks of pyrolytic graphite and by another crystal oriented to specifically remove the  $1.8 \text{ \AA}$  component. Polarisation is achieved by polycrystalline iron filters magnetised to saturation. At  $3.6 \text{ \AA}$  (near the Bragg cutoff) the total cross section for up-spin neutrons is about twice that for down-spin neutrons in the filters. Between the polarising filter and the specimen position there is a Mezei-style neutron spin flipper which can be switched in times of  $1 \mu\text{s}$ . After scattering from the specimen the polarisation is analysed by another iron filter which covers the eight detectors.

Operation proceeds by measuring with flipper on and flipper off. In practice this is done with rapid switching of the spin flipper to facilitate neutron time-of-flight measurements. With the polarising, flipping and analysing efficiencies known, the flipper on and off intensities can be related to the spin-flip (SF) and non-spin-flip (NSF) cross sections of the specimen. By choosing the polarisation direction along the scattering vector all magnetic scattering is with spin-flip (previous paper) and can be isolated.

The isolation of magnetic *diffuse* scattering is particularly important because it invariably is accompanied by other sources of diffuse scattering. Other types of scattering, like magnetic Bragg scattering, can in most cases be identified by other means. Thus a neutron polarisation analysis instrument, like LONGPOL,

is particularly important for other than Bragg magnetic studies and justifies the relaxation in resolution necessary to improve the intensity.

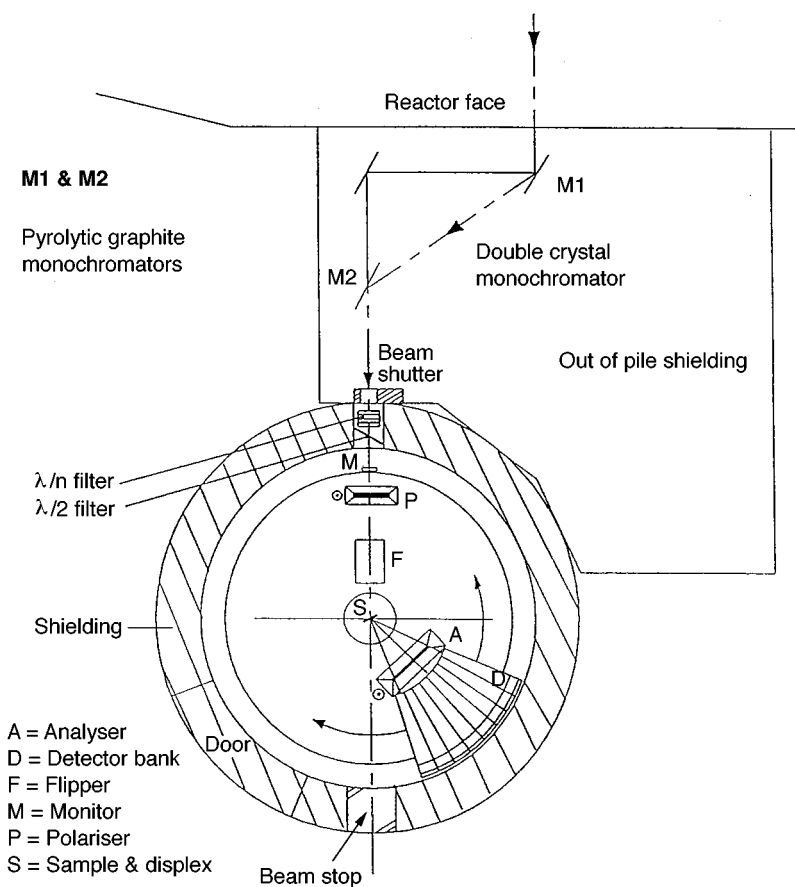


Fig. 1. Schematic diagram of the LONGPOL diffractometer-spectrometer.

### 3. Cu-Mn Spin Glass

Following the identification of the spin glass (Canella and Mydosh 1972) LONGPOL was employed to investigate the magnetic correlations in dilute Mn in Cu alloys. At high temperatures spin glasses are dynamic paramagnets and as such the magnetic neutron scattering is directly related to the imaginary part of the generalised susceptibility, as outlined in the previous paper (Hicks 1997, present issue p. 1119). At low temperatures the dynamics are very slow or frozen. This means that there is opportunity for applying the Kramers-Kronig relations to extract the real part of the generalised susceptibility from the total (energy integrated) neutron cross sections as derived in the previous paper.

Fig. 2 shows the magnetic and nuclear cross sections measured for 5 at% Mn, Cu-Mn. The lower plot shows the magnetic cross sections at various temperatures. The upper plot shows the nuclear cross section which is of course the same for all temperatures. These polycrystalline measurements of the nuclear cross section

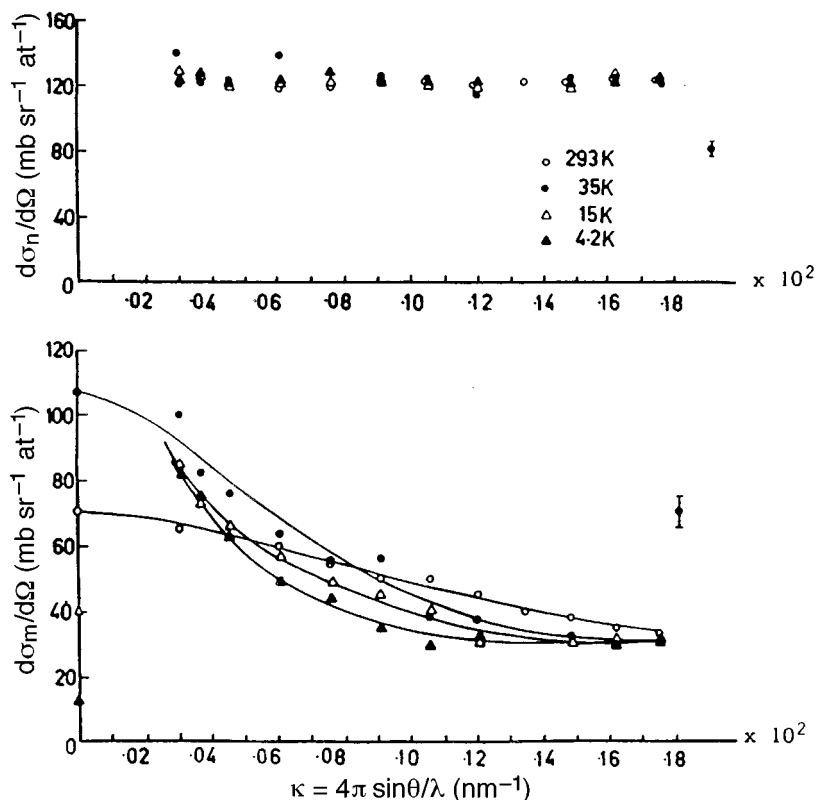


Fig. 2. Nuclear (upper) and magnetic (lower) diffuse scattering from 5 at% Mn Cu-Mn at various temperatures. The nuclear scattering is the product of the virtually random distribution of Cu isotopes and Mn nuclei, the largest part of which is due to the difference between the average Cu nuclear scattering length and the Mn nuclear scattering length. The scattering vector independence of the cross section signifies a random distribution. Above the glass temperature the magnetic cross section extrapolates to a value at zero scattering vector calculated from the magnetic susceptibility. Below the glass temperature the points from susceptibility are much lower than any reasonable extrapolation to zero scattering vector for the reasons discussed in the text.

show no variation with the scattering vector and thus the alloy was assumed to be random. As the scattering lengths for Cu and Mn are very different any overall correlation between the positions of the two atom types would show up as a variation of cross section with scattering vector. The magnetic scattering is seen to be both temperature and scattering vector dependent. For all temperatures the cross section rises towards small scattering vectors, which is characteristic of overall ferromagnetic correlations between Mn moments. This was a surprise as it was assumed that the Mn moments would interact antiferromagnetically as they do for Mn rich Mn-Cu alloys when long range antiferromagnetic order is established.

The magnetic cross sections were also compared with bulk magnetic susceptibility measurements. The cross sections calculated from the susceptibility measurements

are shown at zero scattering vector at each temperature. There is good agreement with a reasonable extrapolation of the neutron cross sections to zero scattering vector except for temperatures below the glass temperature. At these temperatures the points calculated from the susceptibility are too small. This discrepancy can be explained in two ways. It is possible that the glass is still dynamic at the lowest temperatures but that the response time is so long that a normal laboratory measurement is too short for the whole of the susceptibility to be developed. In this case, as the neutron measurement is of the true zero frequency, infinite time susceptibility, it will be larger than the time limited magnetometer measurement. It is also possible that the frozen low temperature state of a spin glass contains a truly static component as is predicted for Ising-type spin glasses. In this case the neutron cross section would contain a truly elastic component unrelated to the susceptibility and again the total neutron cross section would be larger than the magnetometer measurement of the susceptibility. Either way the discrepancy is explained and it is clear that at low temperatures the magnetic response is sluggish with a time constant of at least hours.

To decide between the two alternatives is not easy. Measurements of the magnetic response reveal a time variation mostly close to  $\ln t$  (Mezei and Murani 1979). Such a variation cannot extend to extremely long times and this makes an extrapolation to infinite time impossible.

#### 4. Field Dependent Cross Section of a Cu–Mn Spin Glass

It was surprising that the overall magnetic correlations in Cu–Mn were ferromagnetic from the early experiments. Later experiments (Werner and Cable 1981) extended the magnetic cross section measurements to higher scattering vectors in higher Mn concentration alloys and discovered an increase near to the  $(1, \frac{1}{2}, 0)$  and similar positions. This consisted of a broad maximum at  $(1, \frac{1}{2}, 0)$  with two sharper satellites on the line joining  $(1, 0, 0)$  with  $(1, 1, 0)$ . Whilst quite small in a 5 at% Mn crystal these features become more intense with Mn content. At the same time the small angle evidence for ferromagnetic correlations persists. The question of the connection between the two types of correlation then arises. Do the two types of correlation arise in different parts of the alloy, perhaps a function of the local composition, or do they coexist throughout the alloy? To answer that question we have recently measured the cross section of a 21.4 at% Mn alloy in a field of 4.25 T (Hicks and Cable 1997).

Fig. 3 shows the measured cross sections in the vicinity of the  $(1, \frac{1}{2}, 0)$  position in fields of 0 and 42.5 kOe and at 4.2 K. The cross section measured at 293 K, which is virtually featureless, has been subtracted so that the cross sections displayed are those of the developed magnetic correlations. The measurements were obtained by first cooling to 4.2 K in zero field, taking the zero field measurement, and then warming to 130 K, which is above the glass temperature of approximately 90 K and cooling in 42.5 kOe to 4.2 K and remeasuring. The cross section is reduced by about 10%. It is clear that the field which only interacts with the uniform component of the response (the zero scattering vector response) also reduces the cross section at the  $(1, \frac{1}{2}, 0)$  position which means that these magnetic components are intimately connected with the zero scattering vector or ferromagnetic components. Thus the model of separate ferromagnetic and antiferromagnetic regions is ruled out.

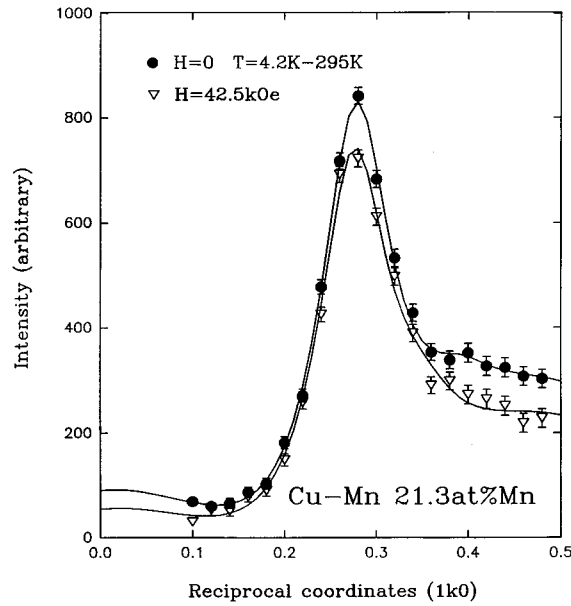


**Fig. 3.** Intensity scattered from a Cu-Mn, 21.3 at% Mn crystal at 4.2 K with the scattering at 295 K subtracted. This is most of the magnetic scattering. After cooling in a field of 42.5 kOe this scattering intensity is reduced by about 10%.

It is interesting to see what sort of entities would result in the decrease of cross section observed. Firstly the reduction is, to a first approximation, the same for all scattering vectors. The exception to this is at the very smallest scattering vectors measured ( $0.08 \text{ \AA}^{-1}$ ) where the reduction is not so much. This means that the scattering might be described as coming from magnetic entities which incorporate both periodicities, in which case we should be able to estimate the size of the entity ferromagnetic moment.

The scattering cross section from a paramagnetic system in the quasielastic approximation is (Hicks 1997)

$$\frac{d\sigma}{d\Omega} = \left(\frac{e\gamma}{\hbar c}\right)^2 [\chi_{xx}(\boldsymbol{\kappa}) + \chi_{zz}(\boldsymbol{\kappa})]k_{\text{B}}T,$$

in which  $\chi(\boldsymbol{\kappa})$  is the wave-vector dependent susceptibility along  $x$  and  $z$  with the scattering vector  $\boldsymbol{\kappa}$  along the orthogonal Cartesian direction  $y$ . The other symbols have their usual meaning. If we assume that the paramagnetic susceptibility is due to superparamagnetic Langevin entities we can write

$$\chi(\boldsymbol{\kappa}) = \frac{N\mu^2 f^2(\boldsymbol{\kappa})}{3k_{\text{B}}T}$$

at zero field, where  $\mu$  is the entity moment and  $f(\boldsymbol{\kappa})$  is its form factor assumed to contain both the ferromagnetic and antiferromagnetic correlations between

individual manganese moments. When a field is applied along the  $z$  direction the appropriate  $z$  component of the susceptibility is the *differential* susceptibility at that field. So we have

$$\chi_{zz}(\boldsymbol{\kappa}) = \left( \frac{dM_z(\boldsymbol{\kappa})}{dH} \right)_H,$$

with the Langevin wave-vector dependent magnetisation

$$M_z(\boldsymbol{\kappa}) = N\mu f(\boldsymbol{\kappa}) \left[ \coth\left(\frac{\mu H}{k_B T}\right) - \frac{k_B T}{\mu H} \right].$$

This gives

$$\chi_{zz}(\boldsymbol{\kappa}) = \frac{N\mu^2 f^2(\boldsymbol{\kappa})}{k_B T} \left[ \frac{1}{\xi^2} - \operatorname{cosech}^2 \xi \right],$$

with  $\xi = \mu H/k_B T$ . For large fields and moments this will be considerably less than the zero field susceptibility leading to the reduction in cross section observed.

The observed reduction in cross section is about 10%. However, this must be due entirely to  $\chi_{zz}(\boldsymbol{\kappa})$  as the contribution to the cross section from  $\chi_{xx}(\boldsymbol{\kappa})$  is unaltered. A 20% reduction in  $\chi_{zz}(\boldsymbol{\kappa})$  corresponds to about  $\xi = 1$ . If we then assume that the characteristic temperature is approximately the glass temperature  $T_g = 90$  K, we can get an estimate for the size of the moment from  $\mu \approx k_B T/H$ . This gives  $36 \mu_B$  per entity. An independent estimate from the width and intensity of the low angle scattering from the ferromagnetic fluctuations gives a similar result.

## 5. Antiferromagnetic Defect Scattering from Mn–Ni

Antiferromagnetic defect scattering arises from the moment defect introduced into an antiferromagnet by a second atomic species. The defect is local, extending only to neighbour atoms close to the defect site. A local defect in real space is composed of a broad range of Fourier components of the magnetic moment. The scattering therefore ranges over a broad range of scattering vectors and is diffuse. This contrasts with magnetic Bragg scattering which is due to the average sublattice moment and is described by a single Fourier component which has a wavelength twice that of the lattice periodicity for a simple antiferromagnet resulting in an intensity at one scattering vector. In a metallic alloy much can be learnt about the electronic structure by the effect of an impurity atom on its surroundings. The difference between this sort of scattering and that from paramagnets and spin glasses is that it is totally elastic because it arises from a static structure. Studies of magnetic defect scattering were firstly made on ferromagnetic alloys and the diffuse magnetic scattering was relatively easily separated by changing the orientation of the moment direction with a field so that the component of the moment perpendicular to the scattering vector is changed and the magnetic cross section is changed. For antiferromagnets this is not possible and neutron polarisation analysis is required to separate the magnetic diffuse scattering.

One of the more comprehensive studies of antiferromagnetic defect scattering done on LONGPOL was that on a 27 at% Ni Mn-Ni single crystal (Moze and Hicks 1982). The results also had a twist to them in that the moment in the defects was found not to be along the direction of the average antiferromagnetic moment.

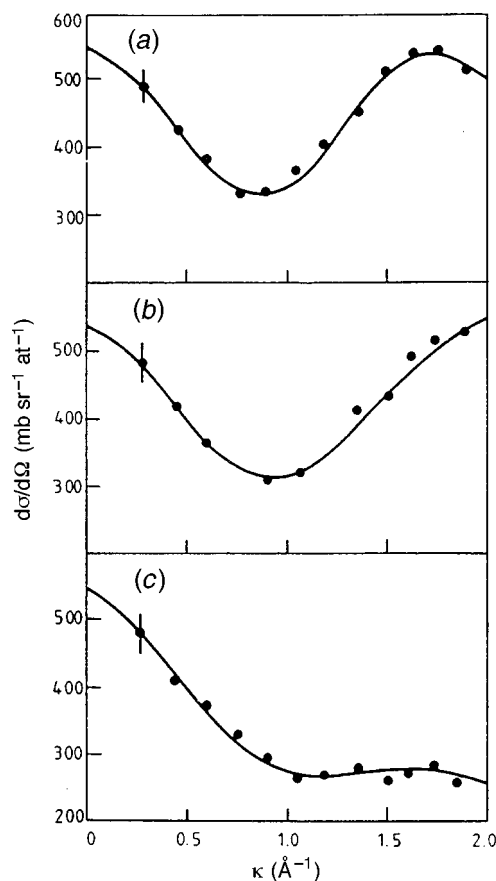


**Fig. 4.** Nuclear disorder scattering cross sections for a  $\gamma$ -Mn<sub>73</sub>Ni<sub>23</sub> crystal along the three principal directions [100], [110] and [111]. The variation of the cross section with scattering vector and direction shows a relatively strong non-random distribution of the atoms. The solid curves are fits to the data which result in pair correlation probabilities for the atom species.

Fig. 4 shows the nuclear diffuse and the magnetic diffuse scattering along the three principal directions of the fcc lattice. The nuclear diffuse scattering, which is sensitive to the correlations between atom positions, shows significant variation with scattering vector. The solid curves are the result of fitting with correlations out to sixth neighbour and the major result is that Mn and Ni atoms are more likely than average to be first neighbours to each other. The magnetic diffuse scattering (Fig. 5) was fitted in a similar way; however, the variation with scattering vector results in parameters describing the effect on

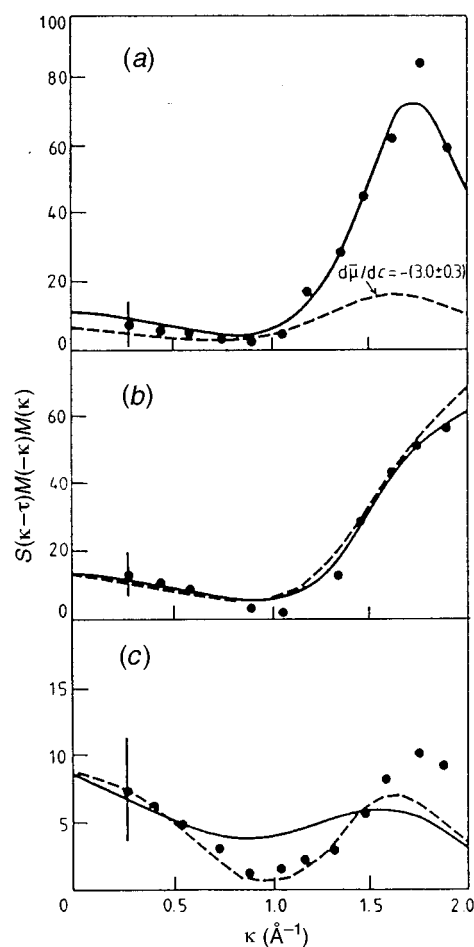


**Fig. 5.** Magnetic diffuse cross sections for a  $\gamma$ -Mn<sub>73</sub>Ni<sub>27</sub> crystal along the three principal directions. The cross sections are plotted in terms of the square of the magnetic defect  $M(\kappa)$  times the atomic distribution function  $S(\kappa-\tau)$  in  $\mu_B^2$ . The solid curve is a free fit to all points. The dashed curve is a fit to all points excluding the large intensity at (001).

neighbouring moments of the presence of an atom of the other species. From the scattering vector independent component it is clear that the Ni carries no moment so that all the other Fourier components relate to the effect of Ni atoms on the moments of the surrounding Mn. The solid curve is an unconstrained fit. It is however unphysical because the total moment defect on the Mn surrounding each Ni atom derived from this fit is far larger than the decrease in average Mn sublattice moment for each additional Ni atom. By eliminating the large peak in the scattering around the (1, 0, 0) position a fit could be obtained (indicated by the dashed curve) for which the resulting defect per Ni atom matched the observed decrease in sublattice moment. Presumably, the extra scattering is due to effects other than the decrease in the *magnitude* of the surrounding Mn moments. The most plausible explanation is that, as this extra scattering is

located only at the  $(0, 0, 1)$  position, which is a reciprocal lattice point for the antiferromagnetic structure, but which is forbidden because of the moment direction of the average structure, the scattering must be due to short range components of the moment transverse to the average moment direction. This explanation has been confirmed in Mn-Cu alloys in which the antiferromagnetic structure is collinear and the antiferromagnetic direction can be preferred. A model describing the local canting has been given by Hicks and Norris (1995).

## 6. Polarised Neutron Time-of-flight Experiments

One advantage of a polarisation analysis experiment is that measurement of neutron time-of-flight is a relatively simple add on, with no loss of total neutron intensity. By using statistical chopping of the incident neutron polarisation a time-of-flight spectrum can be formed which is sensitive to the difference between SF and NSF cross sections.

In Fig. 6 a simple diagrammatic explanation of the technique is given. The spin flipper is pulsed with a time sequence, the self-correlation of which has a triangular peak and a flat background. It is arranged that the pulse sequence is pseudo-random with a known ratio of on-to-off times close to one. The width of the triangular self-correlation peak is proportional to the average period of the impressed sequence. Because of the electronic nature of the switching this can be altered to change one component of the time-of-flight resolution. Part of such a pulse sequence is shown in Fig. 6a. If the scattering is entirely NSF and

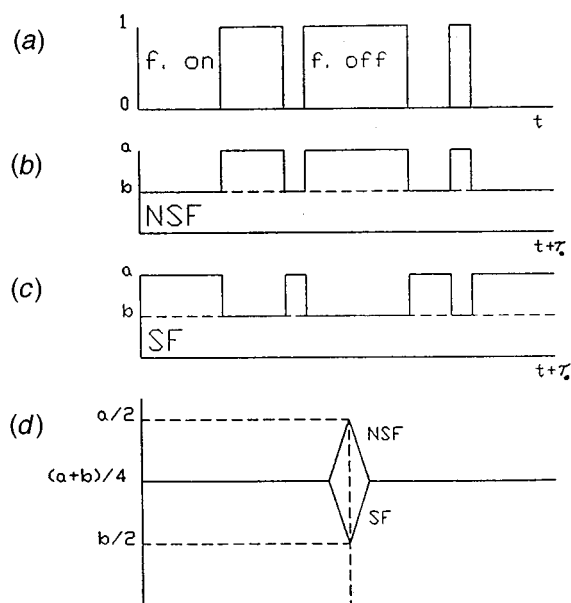


**Fig. 6.** Diagrammatic explanation of the time-of-flight system: (a) part of the pulse sequence sent to the spin flipper; (b) and (c) the resulting time variation of intensity at the detector for purely NSF and SF scattering respectively. Also shown in (d) are simple time-of-flight spectra generated by the cross correlation of impressed and resulting time sequences.

elastic, the impressed pulse sequence will be mirrored in the detected intensity time  $\tau_0$  above a background due to the true background and due to any imperfect polarisation and analysis, as shown in Fig. 6*b*. If the scattering is purely SF and elastic, the resulting detected intensity sequence shown in Fig. 6*c* is the inverse of that for NSF scattering. Cross correlation of the detected intensity sequence with the impressed pulse sequence will yield a peak in the case of NSF scattering, and a dip in the case of SF scattering, at  $\tau_0$  as illustrated in Fig. 6*d*. If the elastic scattering is a mixture of NSF and SF, the peak will be proportional to the difference between them. If the scattering is inelastic there will be a peak or a dip at times other than  $\tau_0$ .

Because there is a background associated with each feature in a time-of-flight spectrum formed by the statistical method, large and sharp features are most easily observed. In particular, in most spectra it is elastic scattering which dominates, so this method is most useful for identifying and measuring the elastic scattering. However, inelastic features are observable and identifiable as being due to SF or NSF processes (Davis *et al.* 1982).

## 7. PrAl<sub>3</sub> Crystal Field Spectra

Crystal field transitions are usefully studied by neutron time-of-flight spectroscopy because the energy levels are virtually dispersionless and all transitions can be seen in the same spectrum. Unpolarised neutron time-of-flight spectroscopy has been used for many years, but there has on occasion been uncertainty about the identification of particular features in the spectrum as crystal field transitions. In many experiments a non-magnetic isomorph of the magnetic material is used to identify possible non-magnetic features in the spectrum. By using time-of-flight with neutron polarisation analysis, as outlined in the last section, magnetic and non-magnetic excitations can be distinguished. In particular, if the polarisation and the scattering vector directions coincide all of the magnetic scattering is SF and is observable as dips in the spectrum.

The material chosen for study was the rare earth trialuminide PrAl<sub>3</sub>. This was selected because of the strength of the transitions and because the transition energies were known (Alekseev *et al.* 1982). This would allow a determination of LONGPOL's ability to make the measurements.

PrAl<sub>3</sub> has a hexagonal Ni<sub>3</sub>Sn-type structure in which the Pr atoms are at sites of hexagonal symmetry D<sub>3h</sub>. The outer electrons are lost to the conduction band, and the nine-fold ground state of the ion is split into three doublets and three singlets by the crystal field of the surrounding ions (Andreef *et al.* 1978). The lowest energy level is a singlet. The ground state transition is of approximately 4.5 meV, with other possibly observable transitions at approximately 3 and 5 meV.

A sample of the material was prepared by melting stoichiometric quantities of Pr and Al together under an ultra-pure argon atmosphere. Neutron diffraction followed by Rietveld fitting showed the sample composition to be approximately 72% PrAl<sub>3</sub>, 14% Pr<sub>3</sub>Al<sub>11</sub> and 6% PrAl<sub>2</sub>, with 8% unidentified. This was considered acceptable, as only the PrAl<sub>3</sub> was likely to give rise to strong SF scattering. Two experimental runs were conducted, one at 295 K and a second at 25 K. Because the intensity, but not the energy measured, depends on angle, the spectra could be summed across detectors to improve the statistics. The spectrum obtained

at 25 K is shown in Fig. 7. The horizontal scale shows energy gained by the scattered neutrons. Visible is a nuclear (NSF) elastic event, and a large SF feature at approximately 4.0 meV. This large feature can be resolved into two peaks, one at 4.5 meV and a second at 3.5 meV on its shoulder. This implies a machine resolution of, at worst, 1 meV which is defined by the width of the elastic peak. An energy of 4.5 meV agrees closely with that from other experiments (Alekseev *et al.* 1982, 1983; Andreef *et al.* 1978), and the lower energy peak has also been seen before (Andreef *et al.* 1978; Alekseev *et al.* 1983). The peaks broaden at 295 K indicating that the broadening is largely due to the width of the transitions themselves, not dispersion, and due in turn to the lifetime of the states.

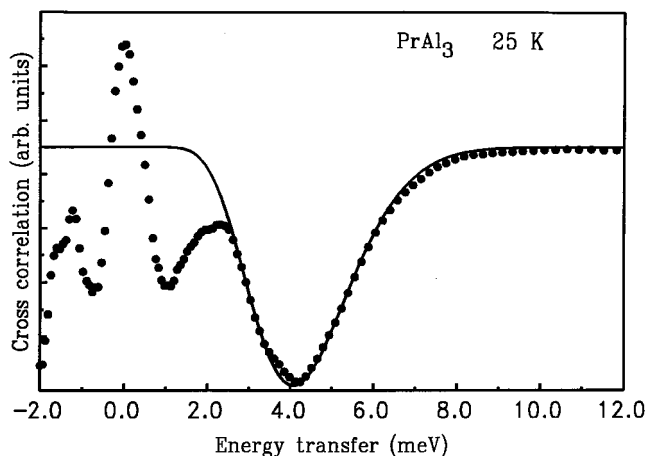


Fig. 7. Crystal field time-of-flight spectrum from  $\text{PrAl}_3$ . Positive going features are from NSF scattering and negative going features from SF scattering. With a polarisation direction along the scattering vector, the magnetic crystal field scattering is with SF. Note the resolution-limited elastic, predominantly NSF peak and the large complex SF peak at about 4 meV, consisting of several crystal field transitions. Note the energy broadened magnetic (SF) scattering at zero energy transfer which results from scattering from the magnetic moments of the excited states.

Of interest is the near elastic scattering. A broadened SF peak is seen superimposed on the truly elastic NSF peak. This peak is due to scattering from the excited states of the Pr atoms. The scattering is quasielastic because of energy uncertainty in the levels, but is not associated with a transition, so energy transfer is centred on zero. The width of this peak gives an indication of the strength of the interaction of the Pr atoms with their environment. Since the central NSF peak has no intrinsic width, being nuclear elastic, this could be used to factor out the width due to machine factors to reveal the interaction strength. This was found to be in the vicinity of 0.4 meV. Further, the machine width was found to be around 0.5 meV, indicating a probable best value for resolution. It can be noted that the peak-within-peak nature of the elastic scattering was made more explicit by the peaks being subtracted rather than added, as would be the case for a conventional unpolarised time-of-flight experiment.

Finally, it is worth noting that because the magnetic scattering is proportional to the imaginary or absorptive part of the susceptibility, the d.c. susceptibility can be obtained by using the Kramers–Kronig relations and integrating over energy (or frequency) and this can be compared with magnetometer measurements.

## 8. Conclusion

This paper has attempted to illustrate two things. Firstly, how the intimate relationship between neutron magnetic cross section and magnetic susceptibility can be used for insight into the behaviour of magnetic systems, either by comparison between neutron experiments and conventional magnetometer measurements or by modelling the cross section using simple concepts based on the understanding of susceptibility. Secondly, how the magnetic neutron cross section can be isolated for such comparisons by the use of neutron polarisation analysis.

## Acknowledgments

The author would like to thank the Australian Institute of Nuclear Science and Engineering and the Australian Research Council for support of this programme of magnetic neutron scattering.

## References

- Ahmed, N., and Hicks, T. J. (1974). *Solid State Commun.* **15**, 415.
- Alekseev, P. A., Sadikov, I. P., Shitikov, Yu. L., Markova, I. A., Christyakov, O. D., Savitskii, E. M., and Kjemis, J. (1982). *Phys. Stat. Sol.* **114**, 161.
- Alekseev, P. A., Goremychkin, E. A., Lippold, B., Mühle, E., and Sadikov, I. P. (1983). *Phys. Stat. Sol.* **119**, 651.
- Andreef, A., Kaun, L. P., Lippold, B., Matz, W., Moreva, N. I., and Walther, K. (1978). *Phys. Stat. Sol.* **87**, 535.
- Cannella, V., and Mydosh, J. A. (1972). *Phys. Rev. B* **6**, 4220.
- Coles, B. R., as referred to by Anderson, P. W. (1970). *Mat. Res. Bull.* **5**, 549.
- Davis, J. R., Cywinski, R., Moze, O., and Hicks, T. J. (1982). *J. Phys. (Paris)* **43**, C7–65.
- Hicks, T. J. (1995). ‘Magnetism in Disorder’ (Oxford Univ. Press).
- Hicks, T. J. (1997). *Aust. J. Phys.* **50**, 1119.
- Hicks, T. J., and Cable, J. W. (1997). *Phys. Rev. B* (submitted).
- Hicks, T. J., and Norris, D. A. (1995). *J. Mag. Magn. Mat.* **140–4**, 1725.
- Mezei, F., and Murani, A. P. (1979). *J. Mag. Magn. Mat.* **14**, 211.
- Moze, O., and Hicks, T. J. (1982). *J. Phys. F* **12**, 1.
- Werner, S. A., and Cable, J. W. (1981). *J. Appl. Phys.* **52**, 1757.